International Journal of Engineering

Journal Homepage: www.ije.ir

Numerical Simulation of Hydrodynamic Properties of Alex Type Gliders

K. Divsalar, R. Shafaghat*, M. Farhadi, R. Alamian

Sea-Based Energy Research Group, Babol Noshirvani University of Technology, Babol, Iran

P A P E R I N F O

Paper history:
Received 04 May 2020
Received in revised form 19 may 2020
Accepted 12 June 2020

Keywords:
Underwater Gliders
Numerical Simulation
Finite Volume Method
Hydrodynamic Coefficients
Angle of Attack

A B S T R A C T

This work presents a numerical Simulation of an underwater glider to investigate the effect of angle of attack on the hydrodynamic coefficients such as lift, drag, and torque. Due to the vital role of these coefficients in designing the controllers of a glider, and to obtain an accurate result, this simulation has been carried on at a range of operating velocities. The total length of the underwater glider with two wings is 900 mm with a 4-digits NACA0009 profile. The fluid flow regime is discretized and solved by computational fluid dynamics and finite volume method. Since the Reynolds number range for this study is in a turbulent flow state (up to 3.7e06), the κ-ω SST formulation was used to solve Navier-Stokes equations and continuity and the angles of attack ranging are from - 8 to 8 degrees. The main purpose of this research is to study the effect of each of the dynamics parameters of glider motion such as velocity and angle of attacks on the hydrodynamic coefficients. Based on the results, the drag and lift coefficients are enhanced with increasing the angle of attack. In addition, the drag coefficient enhanced with increasing the velocity however, when the glider velocity is increased, the lift coefficient does not change significantly except at the highest angle of attack that decreases. The highest drag coefficient is 0.0246, which corresponds to the angle of attack of -8 and the Reynolds number of 3738184. In addition to simple geometry, the glider studied in this paper shows relatively little resistance to flow.

***doi**: 10.5829/ije.2020.33.07a.26*

NOMENCLATURE

A	Reference area (m2)	p	Static pressure (Pa)
L	Reference Length (m)	AoA	Angle of attack (degree)
CD	Drag coefficient (-)	**Greek Symbols**	
CL	Lift coefficient (-)	κ	Turbulence kinetic energy (m2s-2)
CM	Moment coefficient (-)	ν	Kinematic viscosity (m2s-1)
Re	Reynolds number (-)	ρ	Density (kgm-3)
U	Mean stream velocity (m/s)	ω	Specific dissipation rate (s-1)
A	Reference area (m2)	p	Static pressure (Pa)
L	Reference Length (m)	AoA	Angle of attack (degree)
CD	Drag coefficient (-)	**Greek Symbols**	
CL	Lift coefficient (-)	κ	Turbulence kinetic energy (m2s-2)
CM	Moment coefficient (-)	ν	Kinematic viscosity (m2s-1)
Re	Reynolds number (-)	ρ	Density (kgm-3)

1. INTRODUCTION

The exploitation of the oceans and seas is of paramount importance in today's world in terms of transportation, trade, food and pharmaceutical resources, mineral resources and coastal security [1-6]. Underwater glider vehicles are widely used in the monitoring of oceans, exploring and studying various submarine related topics as well as the understanding of global oceanographic phenomena. Therefore, many researchers have investigated the parameters affecting the dynamics of glider motions [7]. They are categorized into three major groups: manned, remote-controlled and automatic underwater gliders [8, 9]. Manned underwater gliders,

*Corresponding Author Institutional Email: *rshafaghat@nit.ac.ir* (R. Shafaghat)

Please cite this article as: K. Divsalar, R. Shafaghat, M. Farhadi, R. Alamian, Numerical Simulation of Hydrodynamic Properties of Alex Type Gliders, International Journal of Engineering (IJE), IJE TRANSACTIONS A: Basics Vol. 33, No. 7, (July 2020) 1387-1396

despite their favorable impact on marine research, are very expensive and time-consuming while gliders, remote control submarines, require less training to control and have fewer security problems. Besides, these types of underwater gliders are capable of onshore controlling and they show high maneuverability needed in surveys over extended periods. The third type of underwater gliders, i.e., automatic underwater gliders, carry their required energy and are capable of performing predefined operations [10]. Underwater gliders are a new generation of automatic gliders that are capable of moving vertically and horizontally underwater by changing their weight. The wings of these gliders help them to propel and control pitch behavior. The unique feature of these gliders is their ability to make exploring missions that take weeks and months. These gliders use buoyancy to propel them and require no further energy. Very low running costs, low power losses and low noise are some of the features that are useful in long time marine surveys. The main purpose of underwater gliders is to obtain information through sensors such as conductivity, temperature and depth gauges that are transmitted to the control center [11].

Over the past few decades, developments in the field of computational fluid dynamics have greatly helped to save costs and to adequately estimate issues such as the study of hydrodynamic behavior [12, 13]. Here are some of the studies that have been done for simulation of underwater gliders. Du et al. [14] presented an analysis of the hydrodynamic characteristics of gliders moving near the ocean floor. The importance of their method is in the glider maneuver, because of changes in vessels hydrodynamic characters near the ocean floor. They later investigated the impact of the underwater glider wings with the help of computational fluid dynamics to determine the effect of glider acceleration and stability [15]. Chen et al [11], hydro-dynamically analyzed a submersible glider for the role of the glider wing in a non-uniform flow. Jung et al. [16] studied the effects of changes in pitch of the propeller and its applications such as backward movement in tunnels. Gao et al. [17] studied a numerical model of a glider with two wings on each side that is angled to the body. The purpose of this research is to investigate and optimize the effect of underwater glider buoyancy motor size on its stability. Barros and Dantas [18] investigated the effect of the ductile propeller glider on the buoyancy forces at different angles of attack and its maneuverability, using κ-ω SST formulation. In a CFD study, they analyzed the combined effect of the control surface deviation and also the angle of attack on the hydrodynamic forces applied to the Pirajuba automated underwater gliders [19]. Ray et al. [20] evaluated the hydrodynamic characteristics of their gliders reaching speeds of up to 6 knots (3 m/s). In their research, the water flow velocity was different from the glider that reached up to 2 knots. Later in a study, Joung et al. [21] optimized the glider geometry to obtain a reduction in the drag coefficient and glider resistance. The hydrodynamic coefficients of a spherical underwater glider for three different types of motions have been investigated by Yu et al. [22]. Zheng et al. [23] studied their capsular underwater glider, using computational fluid dynamics, which has four thrust impellers. Singh et al. [24] also calculated their glider hydrodynamic coefficients using a numerical method and compared them with their experimental results.

Noman et al. [25] extracted their hydrodynamic coefficients, which were almost constant considering the variations in velocity and angle of attack. Lin et al. [26] optimized their 2.7 meters length vessel by using genetic algorithms. In this study, cloud points are obtained from the finite volume simulation method, and by modeling the vessel near the surface they were able to reduce the applied force by 28.9%. Nedelcu et al. [27], were inspired by the body of fish, proposed a glider and calculated the forces acting on it by CFD. Javaid et al. [28] studied the effects of glider wings numerically and experimentally and modeled glider movement in the rotational case. In their research, reducing the wing thickness along its length increases lift force and reduces dynamic stability. Liu et al. [29] applied the hydrodynamic coefficients obtained from the numerical method of rotational motion of the glider with good accuracy according to the experimental results using the dynamic model method. Javaid et al. [30] studied the hydrodynamic properties of their gliders in different conditions. The results of the numerical method were obtained with high accuracy compared to the experimental values.

Here, in this paper, the finite volume method is also used in computational fluid dynamics to study the hydrodynamic behavior of a model of underwater glider at different speeds and angles of attack to investigate the effects of these parameters on the hydrodynamic coefficients such as lift, drag, and torque.

It can be noted that the importance of this study is in the design of the controller for this system which plays an important role in the control and steering of the vehicle.

The remainder of this research is arranged as follows. In section 2, the geometry of underwater glider with a spherical nose is presented. The governing equations and the boundary conditions are derived. In section 3, a finite volume method for numerical solution is developed and the results are discussed. Finally, concluding remarks are provided in section 4.

2. METHOD and ASSUMPTIONS

2. 1. Geometry In this section, after defining the geometry of the glider under study, the assumptions for numerical analysis are given. Figure 1 shows the

geometry of the proposed glider with a spherical nose. The overall length of the glider is 90 cm and its diameter to length ratio is 0.1. The aerodynamic center of the two wings with a 4-digit NACA0012 profile is located 43 cm from its nose tip. As shown in the figure, the width and length of the wings are 12.7 and 39.5 cm, respectively.

2. 2. The Governing Equations The two-equation perturbation model κ-ω SST has been used to analyze the proposed glider [31]. This formulation in the boundary layer portions makes this model directly applicable to the viscous substrate. Therefore, this model can be used as a model of low Reynolds perturbation without any additional damping function. In free flow, the SST formulation changes to κ-ε [32], thereby avoiding the common problem of the κ-ω model, which is sensitive to the perturbation properties of free-flow. In the present model, kinematic eddy viscosity is defined as follows [31]:

$$\vartheta_T = \frac{a_1 \kappa}{\max(a_1\omega, SF_2)} \quad (1)$$

where κ is the perturbation kinetic energy and ω the dissipation rate of this energy. a_1 is a constant value, $S = \frac{\partial u}{\partial y}$ and F_2 a function that adopts a value equal to 1 for boundary layer flow and zero for non-shear stress. The equations used are Navier-Stokes, continuity, and turbulence models, respectively, as follows [33]:

$$\rho\frac{\partial \boldsymbol{u}}{\partial t} + \rho(\nabla\cdot\boldsymbol{u})\boldsymbol{u} = \nabla\cdot[-p\boldsymbol{I} + (\mu+\mu_T)(\nabla\boldsymbol{u} + (\nabla\boldsymbol{u})^T)] \quad (2)$$

$$\rho\nabla\cdot\boldsymbol{u} = 0 \quad (3)$$

$$\frac{\partial\kappa}{\partial t} + U_j\frac{\partial\kappa}{\partial x_j} = P_\kappa - \beta^*\kappa\omega + \frac{\partial}{\partial x_j}\left[(\nu+\sigma_\kappa\nu_T)\frac{\partial\kappa}{\partial x_j}\right] \quad (4)$$

$$\frac{\partial\omega}{\partial t} + U_j\frac{\partial\omega}{\partial x_j} = \alpha S^2 - \beta\omega^2 + \frac{\partial}{\partial x_j}\left[(\nu+\sigma_\omega\nu_T)\frac{\partial\omega}{\partial x_j}\right] + 2(1-F_1)\sigma_{\omega^2}\frac{1}{\omega}\frac{\partial\kappa}{\partial x_j}\frac{\partial\omega}{\partial x_j} \quad (5)$$

The function F_1 is equal to one near the wall and zero at the other.

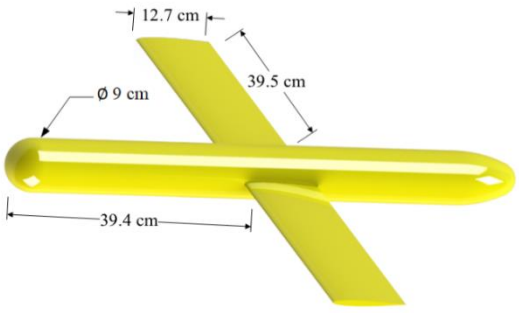

Figure 1. The shape and dimensions of the 90 cm long underwater glider with a spherical nose

Fluid effects on glider generally include drag force (F_D), lift force (F_L), and rotational torque (M), which are used to calculate the drag and lift coefficients, and torque in Equations (6), (7), and (8), respectively [24].

$$C_D = \frac{F_D}{\frac{1}{2}\rho U^2 A} \quad (6)$$

$$C_L = \frac{F_L}{\frac{1}{2}\rho U^2 A} \quad (7)$$

$$C_M = \frac{M}{\frac{1}{2}\rho U^2 Ac} \quad (8)$$

where A is the reference area for calculations, which is considered as the total area of the glider. C_D is the drag coefficient, C_L the lift coefficient, U the mean fluid velocity, and c the length of the airfoil chord.

2. 3. Boundary Conditions The boundary conditions include velocity inlet, turbulent intensity, and turbulent characteristic length for the facing boundaries, zero relative pressure at the output, the symmetry condition for the underwater glider cutting plate, and the non-slip boundary condition for the underwater glider boundaries of the computational environment. It should be noted that the symmetry condition is intended to reduce the computation and its application creates the condition that the same flow pattern appears on the other side of the boundary with acceptable accuracy.

3. Results and Discussion

3. 1. Validation of Numerical Method In order to validate the numerical solution of the present study and to determine the hydrodynamic coefficients of underwater gliders, the studies of Isa et al. [34] were used. In their work, the hydrodynamic coefficients were evaluated by using a Strip theory and a computational fluid dynamics by modeling the k-ω SST turbulence theory with a Reynolds number greater than 10^6 and symmetry boundary condition. It can be noted that in the current research range of Reynolds number is wider than the that of Isa et al. [34]. For assuring the independence of meshing size, three patterns have been chosen. In all of these cases, the angle of attack is about 8 degrees and the velocity of flow is 4.26 m/s (the ultimate condition). These three models have 2.12 million, 3.15 million and 4.01 million elements, respectively. Table 1 shows hydrodynamic coefficients and error values in terms of the third level. As can be seen in Table 1, second level shows accurate results in the time-cost calculation.

The tetrahedron elements are used and the total number of elements in this mesh is 3150396. The pattern used is shown in Figure 2. Modeling the impact of half of the underwater glider on the surrounding flow is considered due to geometrical symmetry. Figure 3

TABLE 1. Results and comparison of different mesh sizes

Grid Level	Grid Number/10^6	Drag Coefficient		Lift Coefficient		Moment Coefficient	
		Value	Error	Value	Error	Value	Error
1	2.12	0.070038	6.7%	0.141256	3.6%	0.005584	7.8%
2	3.15	0.065694	1.6%	0.13633	1.0%	0.005189	2.4%
3	4.01	0.064634	-	0.134951	-	0.005069	-

compares the numerical results of the two methods, which shows the reasonable accuracy of the modeling performed in the present study by the ANSYS-FLUENT R.18.2 commercial software used to solve the flow in the domain.

A comparison of the results of the numerical method with the experimental tests is also provided to ensure the performance of the glider and confirm the accuracy of the simulation. The system needed to perform the test is called the towing tank. Figure 4 shows an overview of the designed glider sample. In addition to the traction system, the towing tank also has data measurement and reporting devices. In order to measure the drag coefficient in different Froude numbers in the towing tank with 38 m long, 3 m wide and 2.5 m deep, the tips of the wings are positioned sufficiently distant from the walls to minimize the effects of the walls on the wing flow. To measure hydrodynamic coefficients, a six-component dynamometer is used. For evaluation of the uncertainty of towing tank system, two types of uncertainty have been evaluated; in this regard, in order to assess the statistical uncertainty, the experiments were repeated 5 times. The overall uncertainty for the towing tank measurement system was evaluated to be 4%. After extracting the coefficients from the experiments, the results are presented along with the numerical simulation results in Figure 5. The convergence criteria is about 10^{-5} in this numerical simulation. As can be seen, the results of both numerical and experimental methods are in good agreement. The maximum error is evaluated to be 9%.

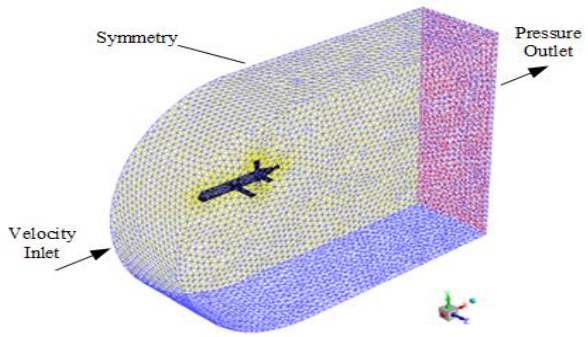

Figure 2. Meshing model investigated by Isa et al. [34] for validation

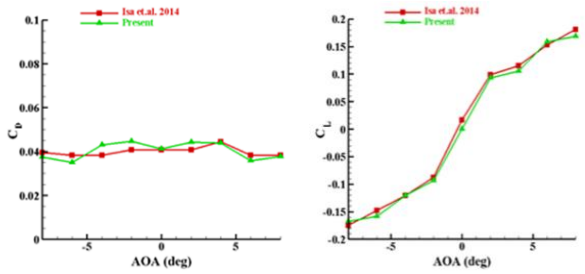

Figure 3. Comparison of the numerical results of the drag and lift coefficient in terms of angle of attack (AOA) at 2.5 m/s

Figure 4. Underwater glider specimen made in a towing tank test

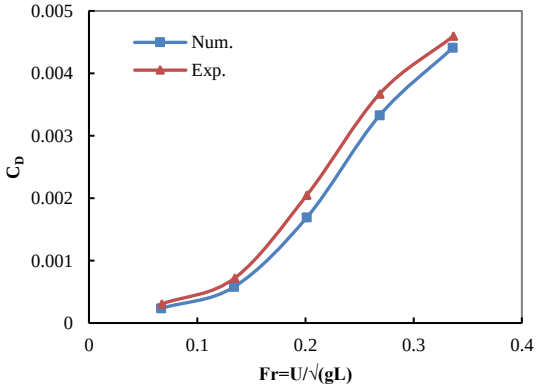

Figure 5. Comparison of numerical and experimental results for different Froude numbers at zero angle of attack

3. 2. Meshing Figure 6 shows the meshing domain for the glider in the present study. The total number of elements in the domain is 3,894,591. Here, as in the model used in validation, symmetry is used and half of the underwater glider is modeled to reduce computation time and cost. As can be seen in this figure, the disorganized tetrahedron mesh is used for analysis. Due to the high gradient in the vicinity of the underwater glider and the turbulence of the stream, the mesh density is considered higher in that area. The diameter of the created domain is 5 times the length of the glider, which is taken to increase the resolution accuracy [22, 25, 35-37].

3. 3. The Effect of Velocity and Angle of Attack The effects of velocity and angle of attack on the drag and lift coefficient for five different Reynolds numbers with values of Re = 747,636.7, 1,495,273, 2,242,910, 2,990,547 and 3,738,184 in terms of 9 different angles of attack from -8 to 8 degrees (intervals 2 Degree) are presented. These values are selected to evaluate the vast range of operating conditions of the proposed glider. As in laboratory conditions, the sample is kept fixed and it moves with its defined velocity at different input angles of attack. Figures 7 and 8 show the glider lift coefficient in terms of angles of attack and velocity, respectively. The two diagrams show that the lift coefficient increases with increasing the angle of attack. However, when the glider velocity is increased, the lift coefficient does not change significantly in all other cases except at the highest angle of attack that decreases.

The drag force coefficients in terms of angle of attack are shown in Figure 9. Based on this figure, at the same angle of attack, the glider drag coefficient enhances by increasing the Reynolds number. The drag force coefficients in terms of velocity are shown in Figure 10. Both figures (Figures 9 and 10) show that the drag coefficient increases with increasing the velocity and the angle of attack. Referring to the graphs, the highest drag coefficient is 0.0246 which corresponds to the angle of attack of -8 and the Reynolds number 3,738,184(equivalent to velocity of 4.26 m/s). On the other hand, the lowest drag coefficient is -0.0084 which corresponds to the angle of attack of 0 and Reynolds number of 747636.7 (equivalent to velocity of 0.852 m/s). The effect of velocity on the drag coefficient is more obvious, indicating that the drag coefficient is more dependent on the velocity compared to the lift coefficient. One of the major parameters that affects the drag force is geometry of the glider and its orientation that can be seen in the differences of drag coefficients at higher angle of attacks such as ± 8 with others in Figure 10.

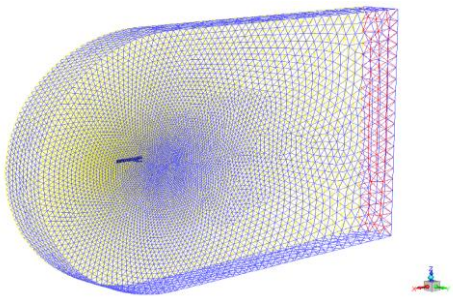

Figure 6. Computational environment and meshing intended for the numerical solution

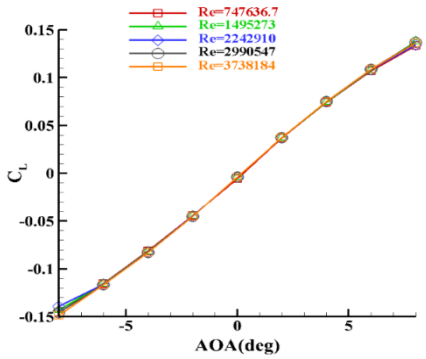

Figure 7. lift coefficient in term of the angle of attack for different flow velocities

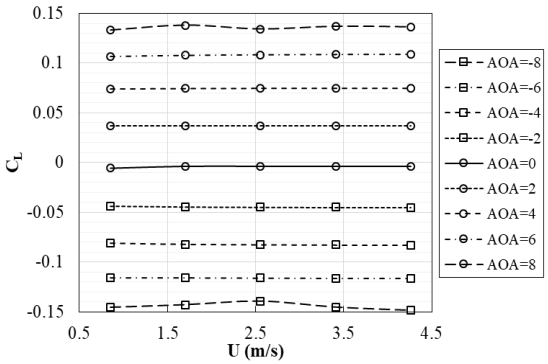

Figure 8. lift coefficient in terms of flow velocity for different angles of attack

Due to specify the oriantation effects in various velocities, the difference of drag coefficient in terms of different attack angles is shown in Table 2.

The results obtained for the presented velocity and angle ranges showed that the drag and lift variations with the angle of attack are higher than the velocity, which indicates the importance of the angle of attack in the hydrodynamic studies. The wings have the most impact on the Lift force and the glider body has the least impact on it. Since the Reynolds number is inversely correlated with the fluid viscosity passing through the vicinity of the body, the viscous forces are less important than the compressive forces and are negligible. So here the drag

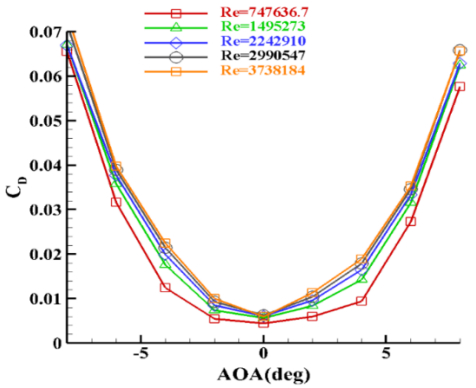

Figure 9. Drag coefficient in terms of angles of attack for different flow velocities

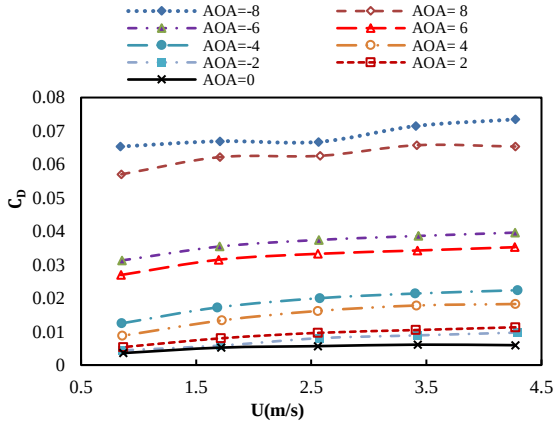

Figure 10. Drag coefficient in terms of flow velocity for different angles of attack

TABLE 2. The percentage difference of drag coefficient in terms of different attack angles

Velocity (m/s)	First angle	Second angle	Percentage difference of drag coefficient
1.7	0	4	156%
	4	8	365%
3.4	0	4	192%
	4	8	269%
4.3	0	4	207%
	4	8	258%

force is dominated by compressive forces. The drag force becomes more important as the angle of attack increases. As the surface area facing the direction of flow increases with increasing angle of attack, the compressive force increases. The torque coefficients in terms of angle of attack and velocity are shown in Figures 11 and 12. As it is shown in these figures, the torque coefficient is distributed approximately symmetrically with the angle of attack, indicating the relative uniformity of the drag and lift forces along with the glider.

3.4. Flow Analysis Around the Glider According to the figures showing the effects of angles of attack on the drag and lift coefficients, as expected, the lift coefficient increases almost linearly with increasing angle of attack.

Due to the low-velocity range, the rate of change of the lift coefficient is low. As shown in Figure 8, the lift coefficient at the angle of attack of 8° is higher than the rest of the glider position due to the decrease in pressure adjacent to the upper surface of the glider wing (Figure 13). Figure 14 shows the flow lines around the glider wing at the angle of 8° and velocity of 4.26 m/s. As shown, the flow hits the airfoil at the angle of 8°, which reduces the pressure at the suction surface and increases the pressure at the pressure surface, thereby, the lifting force increases.

Figure 15 shows that at an angle of attack of 8°, the velocity on the front surface of the glider increases

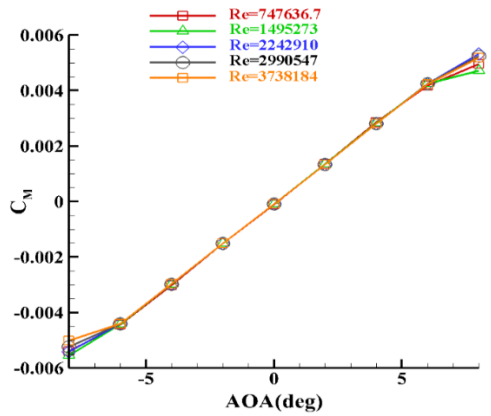

Figure 11. Torque coefficient in terms of angles of attack for different flow velocities

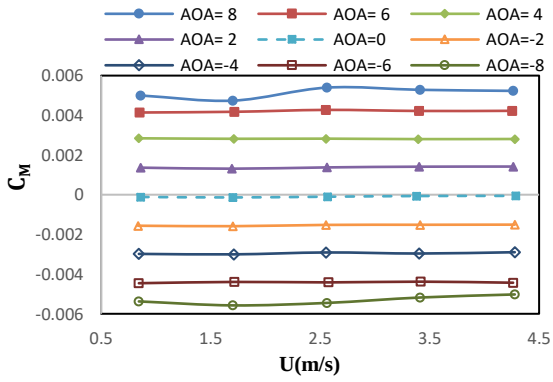

Figure 12. Torque coefficient in terms of velocity for different angles of attack

because of the pressure drop and decreases at the end of the glider. The cause of the deceleration at the end of the glider is illustrated in Figure 16.

Figure 16 illustrates the velocity vector for the angle of attack of 8° and the free-flow velocity of 4.26 m/s. The velocity distribution indicates that velocity is maximum around the underwater glider at the upper part of the nose, and behind the underwater glider, the velocity drops due to vortices.

The static pressure distribution, which represents the pressure applied to the body of the underwater glider, is shown at an angle of attack of 8° in Figure 17. In this figure, the free flow velocity is 4.26 m/s. The pressure is high at the tip of the underwater glider as well as its bottom, which is gradually reduced due to its hydrodynamic geometric shape. The pressure is also high on the front edge and lower part of the glider wings, which is an important factor that increases the lift coefficient at large attack angles. Because of the stagnation point, the maximum pressure is at the tip of the glider's nose. The static pressure is lower for the rest of the glider surface due to the uniform flow between the fluid and the cylindrical body.

Figure 18 illustrates the dynamic pressure distribution (fluid pressure applied to the underwater glider body)

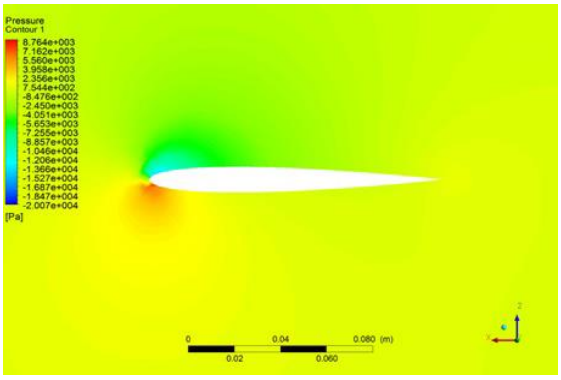

Figure 13. Pressure contour around the glider wing at an 8° angle of attack at the velocity of 4.26 m/s

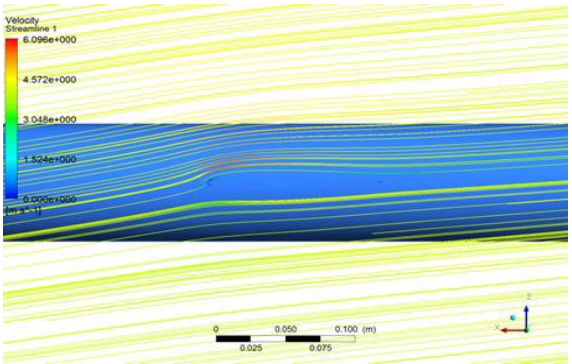

Figure 14. Flow lines around the glider wing at the 8° angle of attack at the velocity of 4.26 m/s

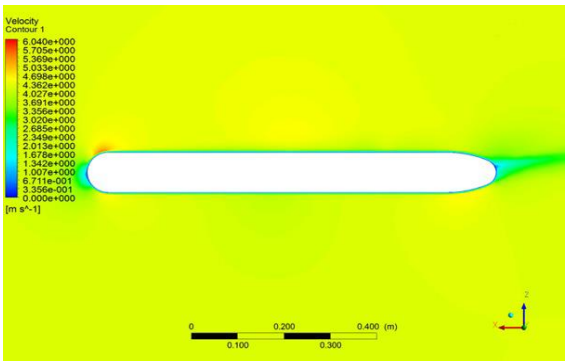

Figure 15. Velocity distribution around the glider body at an attack angle of 8° and a velocity of 4.26 m/s

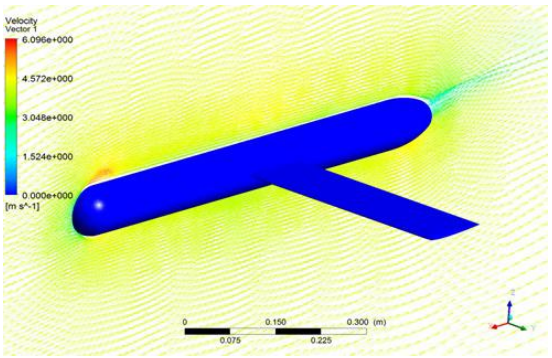

Figure 16. Flow velocity vector around the underwater glider

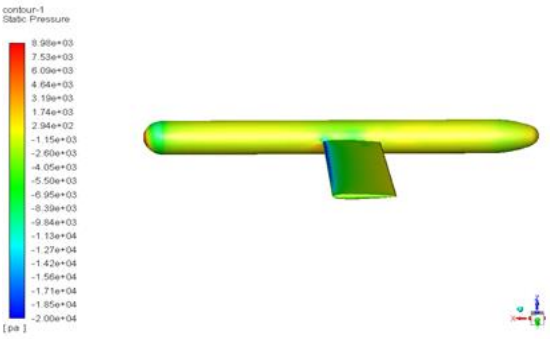

Figure 17. Static pressure contour on the glider body at an attack angle of 8° and a velocity of 4.26 m/s

around the underwater glider. As shown, the front edge of the airfoil experiences the most dynamic pressure. Due to the different dynamic pressure caused by the angle of attack, the lift is created.

The effect of the negative angle of attack on the pressure distribution on the underwater glider is shown in Figure 19, which is obtained for the 8° angle of attack at a velocity of 4.26 m/s. As can be seen, due to the impact of the flow on the underwater glider, most of the pressure is applied to the upper part of the tip and the upper part of the lateral wings. This reduces the lift coefficient.

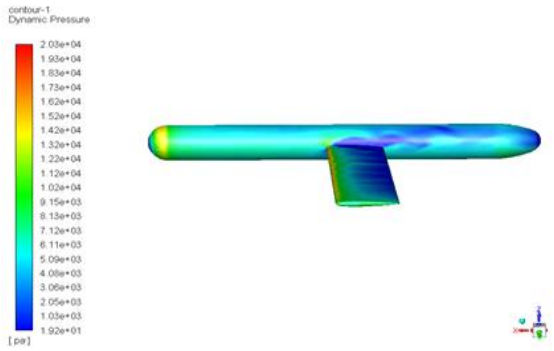

Figure 18. Dynamic pressure distribution on the glider body at an attack angle of 8° and a velocity of 4.26 m/s

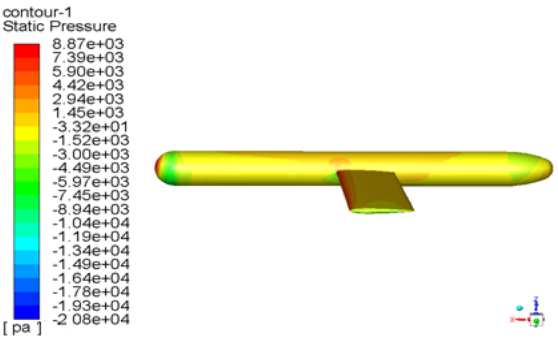

Figure 19. Static pressure contour on the glider body at an attack angle of -8° and a velocity of 4.26 m/s

4. CONCLUSION

In this paper, the numerical analysis of the performance of an automated underwater glider is presented in which numerical simulation has been used to evaluate the hydrodynamic coefficients of the underwater glider (drag, lift, and torque coefficients). In addition, the results also demonstrate the hydrodynamic response of the glider over the velocity and angle of attack. The selected solver method is finite volume. The SST κ-ε perturbation model is used to solve the Navier-Stokes equations and the continuity for fluid velocities up to 4.26 m/s. The accuracy of the method has been verified by comparing it with a similar study as well as with experimental data from testing the actual model. Velocity and pressure field distributions, as well as flow lines, are presented in the results section for underwater glider attack angles from -8 to 8 degrees and different operating velocities. The highest drag coefficient is 0.0246 which corresponds to the angle of attack of -8 and the Reynolds number 3,738,184.The underwater gliders investigated in this paper have suitable hydrodynamic coefficients compared to other gliders, which can be said to reduce the cost due to simpler geometry. This research can be a background for future studies on glider structural analysis and controller design for maneuverability.

5. REFERENCES

1. Alamian, R., Shafaghat, R., Amiri, H.A. and Shadloo, M.S., "Experimental assessment of a 100 w prototype horizontal axis tidal turbine by towing tank tests", ***Renewable Energy***, Vol. 155, (2020), 172-180. doi:10.1016/j.renene.2020.03.139
2. Alamian, R., Shafaghat, R., Bayani, R. and Amouei, A.H., "An experimental evaluation of the effects of sea depth, wave energy converter's draft and position of centre of gravity on the performance of a point absorber wave energy converter", ***Journal of Marine Engineering & Technology***, Vol. 16, No. 2, (2017), 70-83. doi:10.1080/20464177.20462017.21282718.
3. Alamian, R., Shafaghat, R., Farhadi, M. and Bayani, R., "Experimental evaluation of irwec1, a novel offshore wave energy converter", ***International Journal of Engineering, Transactions C: Aspects***, Vol. 29, No. 9, (2016), 1292-1299. doi:10.5829/idosi.ije.2016.29.09c.15
4. Yazdi, H., Shafaghat, R. and Alamian, R., "Experimental assessment of a fixed on-shore oscillating water column device: Case study on oman sea", ***International Journal of Engineering***, ***Transactions C: Aspects*** Vol. 33, No. 3, (2020), 494-504. doi:10.5829/IJE.2020.33.03C.14
5. Alamian, R., Shafaghat, R. and Safaei, M.R., "Multi-objective optimization of a pitch point absorber wave energy converter", ***Water***, Vol. 11, No. 5, (2019), 969. doi:10.3390/w11050969
6. Amiri, H.A., Shafaghat, R., Alamian, R., Taheri, S.M. and Shadloo, M.S., "Study of horizontal axis tidal turbine performance and investigation on the optimum fixed pitch angle using cfd", ***International Journal of Numerical Methods for Heat & Fluid Flow***, Vol. 30, No. 1, (2019), 206-227. doi:10.1108/hff-05-2019-0447
7. Wagawa, T., Kawaguchi, Y., Igeta, Y., Honda, N., Okunishi, T. and Yabe, I., "Observations of oceanic fronts and water-mass properties in the central japan sea: Repeated surveys from an underwater glider", ***Journal of Marine Systems***, Vol. 201, No., (2020), 103242. doi:10.1016/j.jmarsys.2019.103242
8. Leonard, N.E., Paley, D.A., Lekien, F., Sepulchre, R., Fratantoni, D.M. and Davis, R.E., "Collective motion, sensor networks, and ocean sampling", ***Proceedings of the IEEE***, Vol. 95, No. 1, (2007), 48-74. doi:10.1109/jproc.2006.887295
9. Woithe, H.C., Tilkidjieva, D. and Kremer, U., Towards a resource-aware programming architecture for smart autonomous underwater vehicles, in Technical Report DCS-TR-637. 2008, Rutgers University: Department of Computer Science. doi:10.1109/iros.2009.5354098
10. Stommel, H., "The slocum mission", ***Oceanography***, Vol. 2, No. 1, (1989), 22-25. doi:10.5670/oceanog.1989.26
11. Graver, J.G., "Underwater gliders: Dynamics, control and design", Princeton university Princeton, NJ, (2005).
12. Nosrati, K., Tahershamsi, A. and Taheri, S.H.S., "Numerical analysis of energy loss coefficient in pipe contraction using ansys cfx software", ***Civil Engineering Journal***, Vol. 3, No. 4, (2017), 288-300. doi:10.28991/cej-2017-00000091
13. Yamini, O.A., Mousavi, S.H., Kavianpour, M.R. and Movahedi, A., "Numerical modeling of sediment scouring phenomenon around the offshore wind turbine pile in marine environment", ***Environmental earth sciences***, Vol. 77, No. 23, (2018), 776. doi:10.1007/s12665-018-7967-4
14. Du, X.-x., Wang, H., Hao, C.-z. and Li, X.-l., "Analysis of hydrodynamic characteristics of unmanned underwater vehicle moving close to the sea bottom", ***Defence Technology***, Vol. 10, No. 1, (2014), 76-81. doi:10.1016/j.dt.2014.01.007
15. Du, X., Zhang, Z. and Cui, H., "Thrust performance of propeller during underwater recovery process of auv", in OCEANS 2017-

Aberdeen, IEEE., (2017), 1-5. doi:10.1109/oceanse.2017.8084603

16. Jung, H.-J., Kim, M.J., Lee, P.-Y. and Jung, H.-S., "A study on numerical analysis of controllable pitch propeller (CPP) using tunnel inspection auv", in 2012 Oceans-Yeosu, IEEE., (2012), 1-4. doi:10.1109/oceans-yeosu.2012.6263551
17. Gao, L., He, R., Li, Y. and Zhang, Z., "Analysis of autonomous underwater gliders motion for ocean research", in ASME 2014 33rd International Conference on Ocean, Offshore and Arctic Engineering, American Society of Mechanical Engineers Digital Collection., (2014). doi:10.1115/omae2014-24534
18. De Barros, E. and Dantas, J.L.D., "Effect of a propeller duct on auv maneuverability", ***Ocean Engineering***, Vol. 42, (2012), 61-70. doi:10.1016/j.oceaneng.2012.01.014
19. Dantas, J.L.D. and De Barros, E., "Numerical analysis of control surface effects on auv manoeuvrability", ***Applied Ocean Research***, Vol. 42, (2013), 168-181. doi:10.1016/j.apor.2013.06.002
20. Ray, S., Chatterjee, D. and Nandy, S., "Unsteady cfd simulation of 3d auv hull at different angles of attack", ***Journal of Naval Architecture and Marine Engineering***, Vol. 13, No. 2, (2016), 111-123. doi:10.3329/jname.v13i2.25849
21. Joung, T.-H., Sammut, K., He, F. and Lee, S.-K., "Shape optimization of an autonomous underwater vehicle with a ducted propeller using computational fluid dynamics analysis", ***International Journal of Naval Architecture and Ocean Engineering***, Vol. 4, No. 1, (2012), 45-57. doi:10.3744/jnaoe.2012.4.1.044
22. Yue, C., Guo, S. and Li, M., "Ansys fluent-based modeling and hydrodynamic analysis for a spherical underwater robot", in 2013 IEEE International Conference on Mechatronics and Automation, IEEE., (2013), 1577-1581. doi:10.1109/icma.2013.6618149
23. Zheng, H., Wang, X. and Xu, Z., "Study on hydrodynamic performance and cfd simulation of auv", in 2017 IEEE International Conference on Information and Automation (ICIA), IEEE., (2017), 24-29. doi:10.1109/icinfa.2017.8078877
24. Singh, Y., Bhattacharyya, S. and Idichandy, V., "Cfd approach to modelling, hydrodynamic analysis and motion characteristics of a laboratory underwater glider with experimental results", ***Journal of Ocean Engineering and Science***, Vol. 2, No. 2, (2017), 90-119. doi:10.1016/j.joes.2017.03.003
25. Noman, A.A., Tusar, M.H., Uddin, K.Z., Uddin, F., Paul, S. and Rahman, M., "Performance analysis of an unmanned under water vehicle using cfd technique", in AIP Conference Proceedings, AIP Publishing LLC. Vol. 2121, (2019), 040015. doi:10.1063/1.5115886
26. Lin, Y., Yang, Q. and Guan, G., "Automatic design optimization of swath applying cfd and rsm model", ***Ocean Engineering***, Vol. 172, No., (2019), 146-154. doi:10.1016/j.oceaneng.2018.11.044
27. Nedelcu, A.-T., Faitar, C., Stan, L.-C. and Buzbuchi, N., "Underwater vehicle cfd analyses and reusable energy inspired by biomimetic approach", (2018). doi:10.20944/preprints201808.0175.v1
28. Javaid, M.Y., Ovinis, M., Hashim, F.B., Maimun, A., Ahmed, Y.M. and Ullah, B., "Effect of wing form on the hydrodynamic characteristics and dynamic stability of an underwater glider", ***International Journal of Naval Architecture and Ocean Engineering***, Vol. 9, No. 4, (2017), 382-389. doi:10.1016/j.ijnaoe.2016.09.010
29. Liu, Y., Ma, J., Ma, N. and Huang, Z., "Experimental and numerical study on hydrodynamic performance of an underwater glider", ***Mathematical Problems in Engineering***, Vol. 2018, No., (2018). doi:10.1155/2018/8474389
30. Javaid, M.Y., Ovinis, M., Javaid, M. and Ullah, B., "Experimental study on hydrodynamic characteristics of underwater glider", ***Indian Journal of Geo-Marine Sciences (IJMS)***, Vol. 48, No. 7, (2019), 1091-1097.
31. Menter, F.R., "Two-equation eddy-viscosity turbulence models for engineering applications", ***AIAA Journal***, Vol. 32, No. 8, (1994), 1598-1605. doi:10.2514/3.12149
32. Sengupta, A.R., Gupta, R. and Biswas, A., "Computational fluid dynamics analysis of stove systems for cooking and drying of muga silk", ***Emerging Science Journal***, Vol. 3, No. 5, (2019), 285-292. doi:10.28991/esj-2019-01191
33. Boroomand, M.R. and Mohammadi, A., "Investigation of k-ε turbulent models and their effects on offset jet flow simulation", ***Civil Engineering Journal***, Vol. 5, No. 1, (2019), 127. doi:10.28991/cej-2019-03091231
34. Isa, K., Arshad, M. and Ishak, S., "A hybrid-driven underwater glider model, hydrodynamics estimation, and an analysis of the motion control", ***Ocean Engineering***, Vol. 81, No., (2014), 111-129. doi:10.1016/j.oceaneng.2014.02.002
35. Abbas, F.M., "Investigating role of vegetation in protection of houses during floods", ***Civil Engineering Journal***, Vol. 5, No. 12, (2019). doi:10.28991/cej-2019-03091436
36. Ahmad, M., Ghani, U., Anjum, N., Pasha, G.A., Ullah, M.K. and Ahmed, A., "Investigating the flow hydrodynamics in a compound channel with layered vegetated floodplains", ***Civil Engineering Journal***, Vol. 6, No. 5, (2020), 860-876. doi:10.28991/cej-2020-03091513
37. Zhang, S., Yu, J., Zhang, A. and Zhang, F., "Spiraling motion of underwater gliders: Modeling, analysis, and experimental results", ***Ocean Engineering***, Vol. 60, (2013), 1-13. doi:10.1016/j.oceaneng.2012.12.023

Persian Abstract

چکیده

در این مقاله از شبیه‌سازی عددی برای تحلیل ضرایب هیدرودینامیکی گلایدر زیرآبی (ضرایب پسا، لیفت و گشتاور) استفاده شده است. به دست آوردن این ضرایب نقش مهمی در طراحی کنترلر برای هدایت آن دارد. برای انجام این کار، گلایدر زیرآبی در معرض شرایط مختلف عملیاتی اعم از زاویه‌ی حمله و سرعت حرکت آن قرار داده شده است. طول گلایدر زیرآبی ۹۰ سانتی‌متر با دو باله با پروفیل NACA0012 است. سپس، رژیم جریان سیال به کمک دینامیک سیالات محاسباتی و روش حجم محدود گسسته‌سازی و حل شده است. از آن‌جا که محدوده‌ی عدد رینولدز کاری در حالت جریان آشفته است (تا $۳/۷\times۱۰^{۶}$)، از فرمولاسیون $\kappa-\omega$ SST برای حل معادلات ناویر استوکس و پیوستگی بهره گرفته شد. زوایای حمله بررسی شده بین ۸- و ۸ درجه است. هدف اصلی این تحقیق مطالعه‌ی تاثیر هر یک از پارامترهای دینامیکی حرکت گلایدر از جمله سرعت و زاویه‌ی حمله بر ضرایب هیدرودینامیکی است. براساس نتایج، ضریب پسا و بالابر با افزایش زاویه‌ی حمله افزایش می‌یابد. همچنین، با افزایش سرعت، ضریب پسا افزایش می‌یابد، اما با افزایش سرعت گلایدر، ضریب بالابر به جز در بالاترین زاویه‌ی حمله که کاهش می یابد، به طور چشم‌گیری تغییر نمی‌کند. بزرگترین ضریب پسا ۰.۰۲٤٦ است که مربوط به زاویه‌ی حمله‌ی ۸- درجه و مطابق با عدد رینولدز ۳۷۳۸۱۸٤ می‌باشد. گلایدر مطالعه شده در این مقاله علاوه بر هندسه‌ی ساده، در مقابل جریان مقاومت نسبتاً کمی از خود نشان داده است.